“Theoretical Study for Fundamental Properties and Applications of ZnO Nanoparticles”

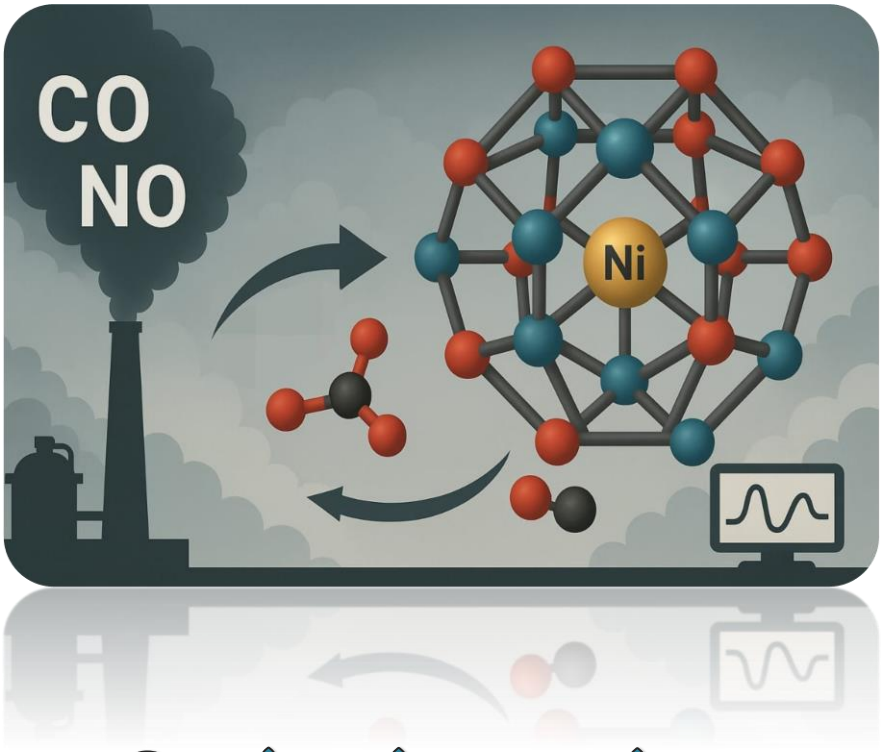

Graduation project 2025_197

Shaza Abdelwahab, Rawda Hassan, Shahd Ayman, Shahd Ahmed,

Menna Muhamed, Marina Meshel

Supervisor: Hayam Osman Taha

Associate Professor of Physics, Ain Shams University, Faculty of Education,

Program: Bachelor’s degree in science and education (Private Physics)

Journal of Applied Research in Science and Humanities

"Theoretical Study for Fundamental Properties and Applications of ZnO Nanoparticles"

Hayam Osman, Shaza Abdelwahab, Rawda Hassan, Shahd Ayman, Shahd Ahmed, Menna Muhamed, Marina Mesheal

Supervisor: **Hayam Osman Taha**

Associate Professor of Physics

Ain Shams University, Faculty of Education, Program Physics

Abstract

Rapid urbanization over the past decade has significantly increased air pollution, posing serious health and environmental risks. Among the most harmful pollutants are carbon monoxide (CO) and nitrogen monoxide (NO). In this study, density functional theory (DFT), using the 6–31G(d) basis set, was used to investigate the adsorption and sensing performance of pristine $Zn_{12}O_{12}$, Ni–$Zn_{12}O_{12}$ (decorated) and $NiZn_{11}O_{12}$ (doped) nanoclusters toward CO and NO gases. The estimated values for the CO and NO molecule adsorption on the Ni–doped cluster are –1.63 eV and –1.505 eV, respectively. Also, the electronic sensitivity of pure $Zn_{12}O_{12}$ nanoclusters decorated with Ni to CO and NO gas was investigated. It was found that adding the Ni atom to pristine $Zn_{12}O_{12}$ changed the cluster sensitivity. The estimated values for the CO and NO molecule adsorption on the Ni–decorated cluster are –3.104 eV and –3.044 eV , respectively. These studies demonstrated that Ni–$Zn_{12}O_{12}$ and $NiZn_{11}O_{12}$ nanoclusters can be suggested as an effective choice for gas sensors that can identify CO and NO gases. Additionally, the computation results from CO and NO adsorption on Ni– $Zn_{12}O_{12}$ nanocluster indicates that Ni–$Zn_{12}O_{12}$ nanocluster has the most potential to improve the accuracy and reliability of hazardous substances, such as NO, and CO, detection in next–generation sensor technologies.

Keywords

Ni–doped; DFT; Gas sensors; ZnO nanocage; $Zn_{12}O_{12}$

1. Introduction

The past ten years have seen a sharp increase in air pollution due to the world's cities growing so quickly globe (Zhuiykov et al., 2001, 484; Chang et al., 2001, 3863). This results in a serious environmental health issue that impacts individuals. Environmental gas monitoring and management acknowledged as a crucial area for clean air and human health since air pollution is a mixture of solid particles and gases in the air that include dangerous and damaging vapors (Gupta and Nayak, 2012, 81; Mittal et al.,2009, 345). Usually, poisonous compounds including carbon monoxide (CO), dangerous gases, and very small particles are released as a result (Ferroni et al., 1998, 285; Sberveglieri G. et al., 1995, 89; Gurlo A. et al., 1998, 92). Two of the most harmful substances found in air pollution and everyday life are carbon monoxide (CO) and nitrogen oxide (NO). Therefore, for environmental measures and controls, efficient techniques to identify and reduce the CO and NO concentration in the atmosphere have been extensively sought after (Santucci et al., 2003, 10904–10910; Lee et al., 1999, 57). Carbon monoxide (CO), a colorless and odorless petrol with high toxicity, is mostly generated when fuels burn incompletely. Additionally, because CO interacts poorly with most sensors, reorganizing it is one of the difficult problems associated with it. (Peyghan et al., 2013, 859; Omaye, 2002, 180; Beheshtian et al., 2011, 1400; Beheshtian et al., 2011, 546; Beheshtian et al., 2012, 71). Nanowires, nanotubes, nanoribbons, nanobelts, nanorings , nanoclusters, and other nanostructures are among the most abundant in ZnO. For the detection of several gases, including NH_3, NO, F_2, O_2, and CO, these ZnO nanostructures have frequently been used as gas sensors (Lahmer, 2016,89; Peyghan, Noei, (2013), 231; Peyghan et al., 2015, 1233; An et al., 2008, 5747). Non–metal ion doping and vacancy–defect creation are employed in sensing applications to improve the electrical characteristics and electron transport by manipulating the substrate materials' shape and overcoming their poor sensitivity (Özgür et al., 2005, 041301). Because of its special qualities, such as its large exciton binding energy (60 meV) at room temperature, its wide bandgap (3.44 eV at 4.2 K), its transparency in the visible spectrum, its non–toxicity, and its biocompatibility, zinc oxide (ZnO) is currently one of the most significant semiconductors for a variety of applications in nanodevices (Özgür et al., 2005, 041301). Since fullerene–like nanoclusters have distinctive qualities that make them useful for a range of applications, such as photocatalysis, solar cells, gas sensors, or hydrogen storage, they require particular attention among a wide range of nanostructures (Beheshtian et al., 2012, 115–118; Sebastian , Ocamp, 1996, 1–10;

Chakrabarti et al., 2000, 113). (Gorgani et al.,2016,1573) investigated the adsorption of carbon monoxide (CO) and nitrogen monoxide (NO) on heterogeneous $C_{16}Zn_8O_8$ using a computational method. It was found that CO could adsorb on $C_{16}Zn_8O_8$ via chemisorption mechanism with E_{ads} of –0.74 eV, which further stabilized the complex system. In fact, the adsorption of CO reduced the E_g of the cluster, making it a sensitive sensor. According to earlier research, $(ZnO)_{12}$ nanoclusters have been effectively synthesized (Yadav et al.., 2007, 195450) and are the most stable hollow structure for the tiny cluster . (Wang et al., 2007, 4956; Reber et al., 2007, 221). Since ZnO nanostructured materials are plentiful, safe, and simple to manufacture, they have been thoroughly investigated as chemical sensors (Beheshtian et al., 2012, 8171; Galstyan et al., (2015),14239–; Peyghan et al., 2014, 566; Ameen et al., 2016, 562; Peyghan et al., 2014, 105; Rocha et al., 2016, 4539; Peyghan et al., 2015, 1233; Salimi et al., 2015, 609). Doping the structure of ZnO with various metal atoms, such as Ga, Cu, In, Sn, Au, etc., is a popular method to boost the reactivity and sensitivity of pristine ZnO nanoparticles, which typically have limited sensitivity towards chemicals (Shirini et al., 2015, 123; Benramache et al., 2013, 1; Hongsith et al., 2008, 823; Sahay et al., 2008, 654). (Saeed Aslanzadeh, 2016, 160) use a ZnO nanocage ($Zn_{12}O_{12}$) as a model for ZnO nanomaterials and investigate how the sensitivity of $Zn_{12}O_{12}$ to CO changes when a Zn atom swapped out for transition metals such as Sc, V, Ti, Cr, Mn, and Fe. they investigated the behavior of several doped and pristine ZnO clusters in the presence of CO molecules using calculations from density functional theory. In researches (Saeed Aslanzadeh, 2016, 160; Mariya Kovalenko et al., 2020, 790; An W et al., 2008, 5747; Zhihong et al., 2020; Liangruksa et al., 2021, 148868) the structural, electronic, and adsorption properties of zinc oxide doped with a different set of elements (Sc , Ti , Mn , Fe , Cr , Pt , V) were studied during the five researches towards CO and NO gas. They were used as chemical sensors. In the case of doping zinc oxide with chromium, it was found to be more efficient and effective than pure zinc oxide. Consequently, zinc oxide doped with chromium was used in remote sensing devices towards carbon monoxide, which led to a change in energy gap that caused a change in electrical conductivity. It can be concluded from this that doping improves the conductivity and adsorption of nano groups.

In the current study, a DFT technique was used to investigate the effects of CO and NO molecule adsorption on the electrical and geometrical properties of pure $Zn_{12}O_{12}$ in addition to decorated ZnO (Ni– $Zn_{12}O_{12}$) and doped Ni– $Zn_{11}O_{12}$. All structures' electrical properties, energy parameters, and geometric

optimization were investigated using natural bond orbitals (NBOs). All geometry optimization calculations were performed using DFT with the B3LYP and 6–31G(d) basis set. The intermolecular interactions between gas molecules and the aforementioned nanocages were examined.

2. The Computational Methods

Energy calculations, geometry optimizations, and natural bond orbital analyses performed on the pristine $Zn_{12}O_{12}$, Ni–$Zn_{12}O_{12}$ (decorated) and Ni–doped $Zn_{11}O_{12}$ clusters and their complexes with CO and NO molecules. The Gaussian 09 suite of algorithms used to optimize the geometry of all the compounds under investigation, with no symmetry restrictions. (Frisch, et al., 2009). For geometry optimization, the exchange–correlation functional of Becke–3–Lee–Yang–Parr (B3LYP) (Becke, 1993, 1372). In each instance, the geometries optimized using the 6–31G(d) basis set, and the single point energy was subsequently computed using the same basis set. We have defined adsorption energy in the usual way as:

$$E_{ads} = E_{gas/Zn_{12}O_{12}} - (E_{Zn_{12}O_{12}} + E_{gas}) \quad (1)$$

$$E_{ads} = E_{gas/NiZn_{12}O_{12}} - (E_{NiZn_{12}O_{12}} + E_{gas}) \quad (2)$$

$$E_{ads} = E_{gas/NiZn_{11}O_{12}} - (E_{NiZn_{11}O_{12}} + E_{gas}) \quad (3)$$

Where, $E_{gas/Zn_{12}O_{12}}$, $E_{gas/NiZn_{12}O_{12}}$, $E_{Zn_{12}O_{12}}$, $E_{NiZn_{12}O_{12}}$, and E_{gas} are the energies for the ($E_{gas/Zn_{12}O_{12}}$, $E_{gas/NiZn_{12}O_{12}}$) complex, ($E_{Zn_{12}O_{12}}$, $E_{NiZn_{12}O_{12}}$) substrate, and free gases, respectively. HOMO–LUMO gap (Eg) defined as:

$$E_g = E_{LUMO} - E_{HOMO} \quad (4)$$

where E_{LUMO} and E_{HOMO} are energies of highest occupied molecular orbital (HOMO) and lowest unoccupied molecular orbital (LUMO). To further investigate the stability and reactivity of the $Zn_{12}O_{12}$, gases/ $Zn_{12}O_{12}$, Ni–doped $Zn_{11}O_{12}$, and gases/Ni–doped $Zn_{11}O_{12}$ nanocages, global reactivity descriptors considered. The ionization potential (IP) and electron affinity (EA) in Equations (5) and (6), respectively.

Ionization potential (IP, eV)

$$Ip = -E_{Homo} \quad (5)$$

electron affinity (EA, eV)

$$EA = -E_{LUMO} \quad (6)$$

At T = 0 K, the Fermi level (E_F) energies computed (Ernzerhof, 2009, 793; Islam, Ghosh, 2011, 135). Where anticipated to be:

$$E_F = (E_{LUMO} + E_{HOMO})/2 \quad (7)$$

Chemical softness (S), chemical potential (μ), electrophilicity (ω), and chemical hardness (η) can also be calculated using equations 8, 9, 10 and 11 based on (Chattaraj, Roy, 2007, 46)

softness (S, eV^{-1}),

$$S = \frac{1}{2\eta} = \frac{1}{(IP-EA)} \quad (8)$$

chemical potential (μ, eV)

$$\mu = -\frac{(IP + EA)}{2} \quad (9)$$

the electrophilic index (ω, eV)

$$\omega = \frac{\mu^2}{2\eta} \quad (10)$$

chemical hardness (η, eV)

$$\eta = \frac{1}{2}(IP - EA) \quad (11)$$

Gauss View 5.0 software used to visualize the optimal geometries (Dennington R. et al, 2009).

3. Results of Research

Table 1: Structural and energetic parameters of the optimized $Zn_{12}O_{12}$, CO, and NO adsorbed on $Zn_{12}O_{12}$ nanocages. All distances (d, Å), adsorption energies ($\Delta E_{ads.}$, eV), and dipole moment (D, Debye).

System	$\Delta E_{ads.}$	d (O -XO)	d (Zn -XO)	$D_{(X-O)}$	D
$Zn_{12}O_{12}$	-	-	-	-	0.0373
CO	-	-	-	1.138	0.0598
NO	-	-	-	1.1587	0.0886
CO/ $Zn_{12}O_{12}$	-0.215	4.115	3.407	1.141	1.6125
NO/ $Zn_{12}O_{12}$	-0.047	2.654	3.243	1.165	0.6889

Table 2: Structural and energetic descriptors of the optimized CO, and NO adsorbed on ($NiZn_{12}O_{12}$ and $NiZn_{11}O_{12}$) nano–cages. All distances (D, Å), The adsorption energy ($\Delta E_{ads.}$, eV), (E_H, eV), (E_L, eV), (E_g, eV), NBO charges (Q, |e|) and dipole moment (D, Debye). ($\Delta E_{ads.}$) calculated at the DFT/B3LYP–GD3/6–31G (d) level of theory

System	$E_{ads.}$	$d_{(Ni-Zn)}$	d (Ni -O)	d (Ni -XO)	$d_{(X-O)}$	Q_{Ni}	Q_{Zn}	Q_O	D
$NiZn_{12}O_{12}$	-6.139	2.238	1.714	-----	----	0.437	0.7755	-1.140	2.208
$CO/NiZn_{12}O_{12}$	-3.104	2.229	1.783	1.672	1.161	0.3695	0.969	-1.1886	1.607
$NO/NiZn_{12}O_{12}$	-3.044	2.245	1.784	1.633	1.184	0.417	0.495	-0.569	1.953
$NiZn_{11}O_{12}$	-----	-----	1.825 1.826	------	------	0.8798	1.26	-1.108	1.662
$CO/NiZn_{11}O_{12}$	-1.63	-------	1.889 1.851	1.776	1.141	0.686	1.269	-1.126	0.761
$NO/NiZn_{11}O_{12}$	-1.505	-------	1.907 1.880	1.792	1.161	0.204	0.632	-0.560	0.566

Table 3: (HOMOs) (EH, eV), (LUMOs) (EL, eV), (HOMO–LUMO) energy gap (Eg, eV), Fermi level (Ef, eV), electron affinity (EA, eV), Ionization potential (IP, eV), chemical hardness (η, eV), softness (S, eV^{-1}), chemical potential (μ, eV) and the electrophilic index (ω, eV) of $Zn_{12}O_{12}$, free gases, CO,NO/ $Zn_{12}O_{12}$ and TM – $Zn_{12}O_{12}$ nanocages.

System	E_H	E_L	Eg	E_F	IP	EA	η	S	μ	ω
$Zn_{12}O_{12}$	-6.985	-2.855	4.13	-4.92	6.985	2.855	2.065	0.242	-4.92	5.861
NO	-5.878	-2.857	3.020	-4.368	5.878	2.857	1.511	0.331	-4.368	6.312
CO	-10.095	-0.593	9.502	-5.344	10.095	0.593	4.751	0.105	-5.344	3.006
CO/ $Zn_{12}O_{12}$	-6.846	-2.718	4.128	-4.782	6.846	2.718	2.064	0.242	-4.782	5.539
NO/ $Zn_{12}O_{12}$	-5.967	-3.211	2.756	-4.589	5.967	3.211	1.378	0.363	-4.589	7.641
Ni $Zn_{12}O_{12}$	-5.592	-2.749	2.844	-4.171	5.592	2.749	1.4215	0.352	-4.171	6.12
CO/Ni$Zn_{12}O_{12}$	-6.193	-2.878	3.316	-4.536	6.193	2.878	1.658	0.302	-4.536	6.205
NO/Ni$Zn_{12}O_{12}$	-6.453	-2.897	3.556	-4.675	6.453	2.897	1.778	0.281	-4.675	6.146
Ni $Zn_{11}O_{12}$	-6.108	-2.853	3.255	-4.481	6.108	2.853	1.628	0.307	-4.481	6.166
CO/Ni$Zn_{11}O_{12}$	-6.487	-2.777	3.710	-4.632	6.487	2.777	1.855	0.269	-4.632	5.783
NO/Ni$Zn_{11}O_{12}$	-6.428	-3.328	3.100	-4.878	6.428	3.328	1.55	0.323	-4.878	7.676

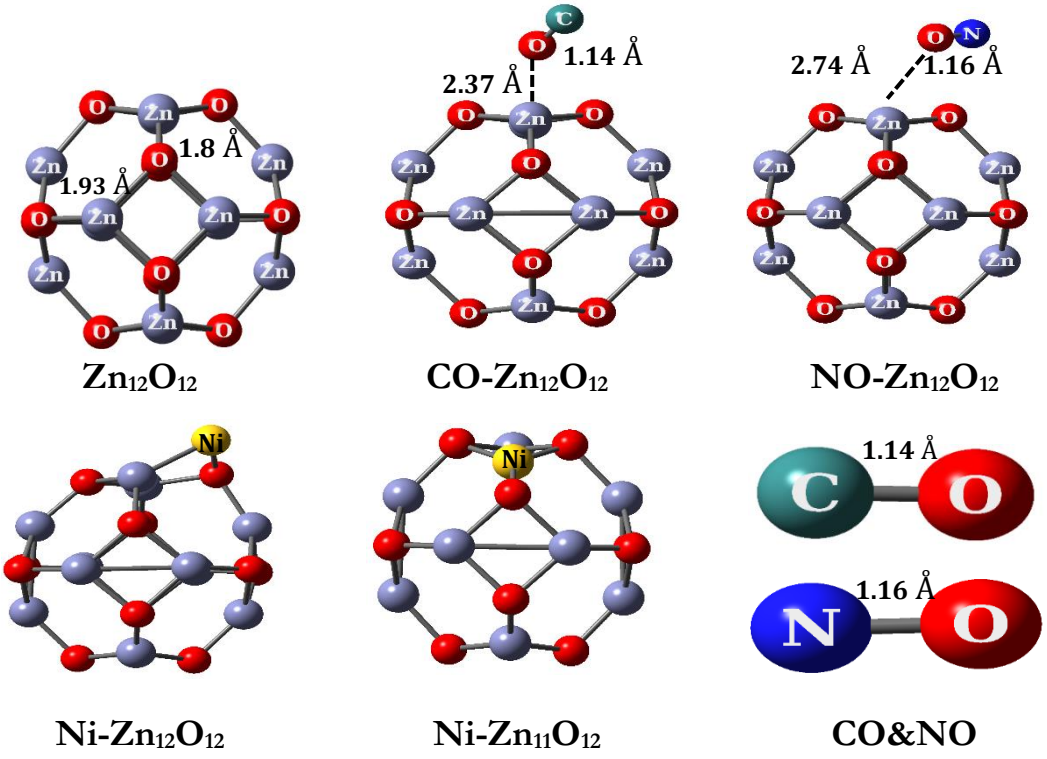

Fig. 1. The optimized structures of $Zn_{12}O_{12}$, CO–$Zn_{12}O_{12}$, NO–$Zn_{12}O_{12}$, Ni–$Zn_{12}O_{12}$, Ni–$Zn_{11}O_{12}$ nanocages, and (NO & CO) gases at (DFT/B3LYP/6–31G(d)). Atoms are labelled as seen above.

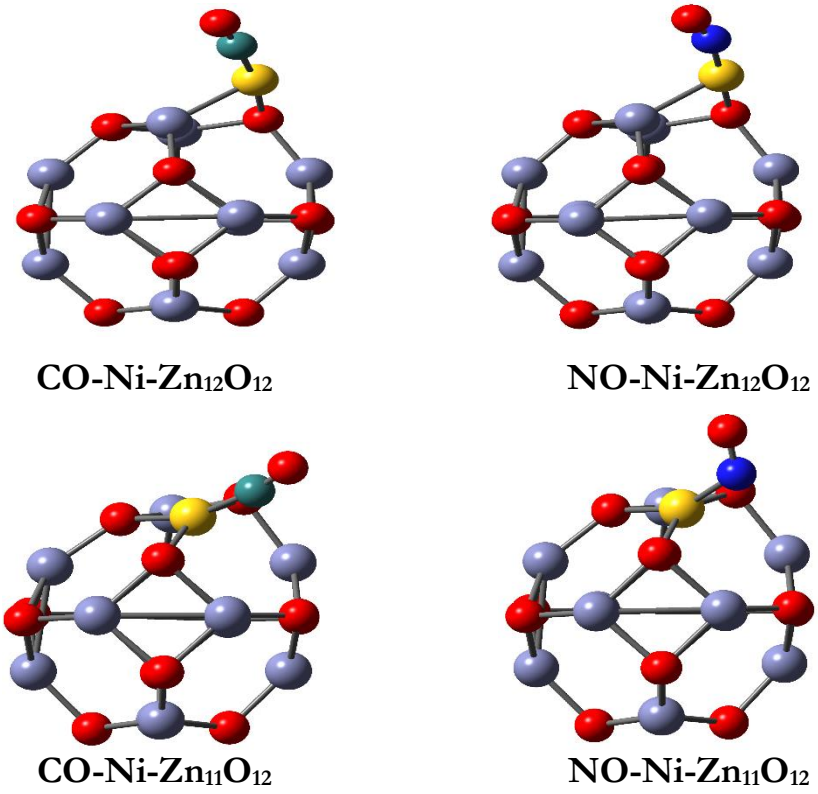

Fig. 2. The optimized structures of CO–Ni–$Zn_{12}O_{12}$, NO–Ni–$Zn_{12}O_{12}$, CO–Ni–$Zn_{11}O_{12}$, and NO–Ni–$Zn_{11}O_{12}$ nanocages, NO & CO gases at (DFT/B3LYP/6–31G(d)).

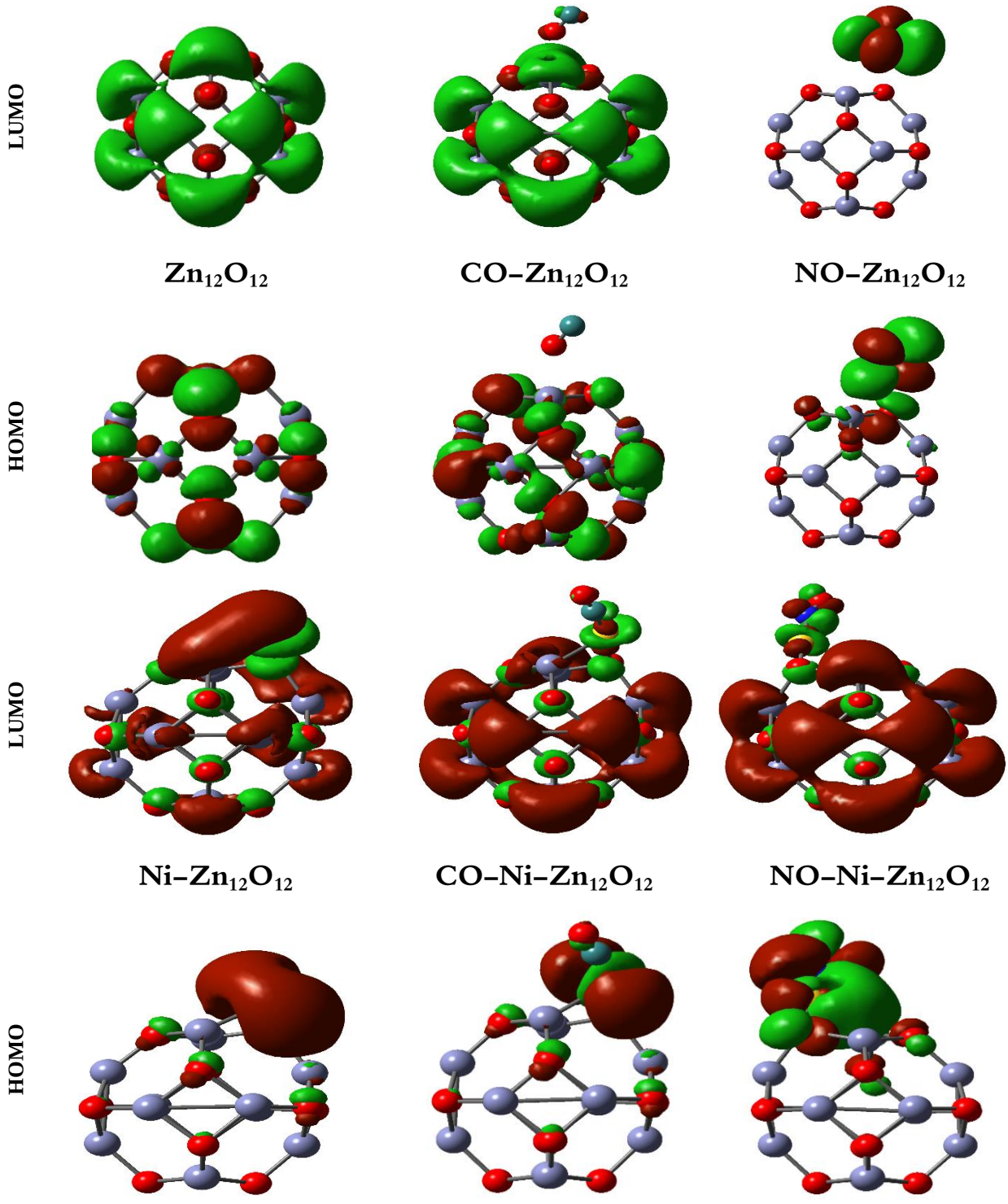

Fig. 3: Frontier orbital isosurface plots of $Zn_{12}O_{12}$, $CO–Zn_{12}O_{12}$, $NO–Zn_{12}O_{12}$, $Ni–Zn_{12}O_{12}$, $CO–Ni–Zn_{12}O_{12}$, and $NO–Ni–Zn_{12}O_{12}$ (at isovalue 0.02).

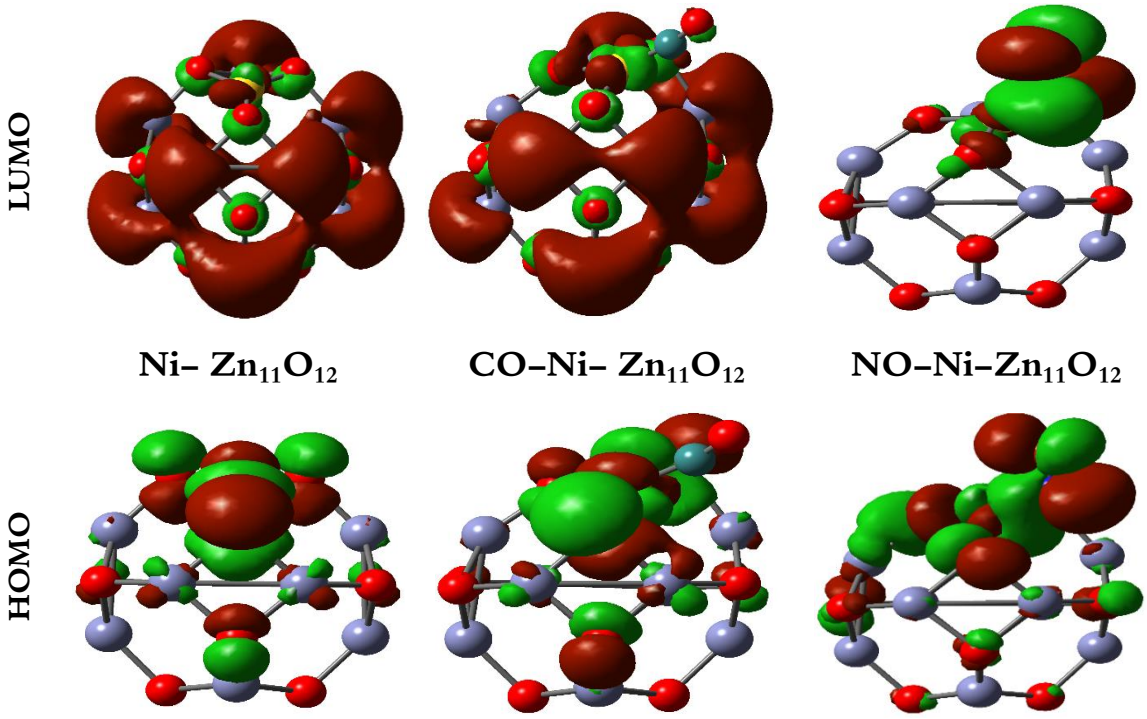

Fig. 4: Frontier orbital isosurface plots of Ni– $Zn_{11}O_{12}$, CO–Ni– $Zn_{11}O_{12}$, and NO–Ni– $Zn_{11}O_{12}$ (at isovalue 0.02).

4. Interpretation of Results

4.1 Interaction of CO and NO with $Zn_{12}O_{12}$

Using DFT, we first examined the relaxed structure of pure $Zn_{12}O_{12}$, which has 12 zinc and 12 oxygen atoms. The ZnO cage's optimized shape depicted in Figure 1, which reveals that it has eight hexagon and six tetragon rings. Prior to optimization, one of the bonds is about 2.20 Å, shared between two hexagons, while the other has a length of 2.27Å, shared between a tetragon and hexagon. Following optimization, two distinct Zn–O bonds decreased: one has a length of about 1.93 Å, shared between two hexagons, while the other has a length of 1.85 Å, shared between a tetragon and hexagon. The optimized geometries of $CO/Zn_{12}O_{12}$ and $NO/Zn_{12}O_{12}$ presented in Figure 1.

4.2. Interaction of (CO & NO) with ($NiZn_{12}O_{12}$ & $NiZn_{11}O_{12}$)

The transition element, nickel, incorporated in two ways: by doping and decoration.

4.2.1. Decorated ZnO:

One transition metal atom, Zn, decorated with another transition metal atom, Ni, to evaluate $Zn_{12}O_{12}$'s sensitivity to the CO and NO molecules. The structures that have optimized (Figures 1 and 2). which are different from the pristine cluster's. For Ni–decorated nanoclusters, structural geometry changes. In this instance, the values of d_{Ni-Zn}, and d_{Ni-O} are (2.23 and 1.71) Å, respectively. By investigating the CO molecule's adsorption on decorated $NiZn_{12}O_{12}$, from Table 2, decorating a Zn atom with Ni atom gives highest negative adsorption energy. The $CO/NiZn_{12}O_{12}$ adsorption energy is approximately –3.104 eV, which is approximately 2.889 eV higher than the CO adsorption energy on the pristine cluster. By investigating the NO molecule's adsorption on decorated $NiZn_{12}O_{12}$, from Table 2, $NO/NiZn_{12}O_{12}$ gives highest negative adsorption energy (–3.044 eV), which is approximately 2.997 eV higher than the NO adsorption energy on the pristine cluster. We conclude that $Ni–Zn_{12}O_{12}$ nanocage has the potential to improve the accuracy and reliability of hazardous material detection, such as NO and CO.

4.2.2. Doped ZnO

One transition metal atom, Zn, replaced by another transition metal atom, Ni, to investigate the change in $NiZn_{11}O_{12}$'s sensitivity to the CO and NO molecules. The optimized structures under study shown in (Figures 1 and 2). Ni–dopped nanoclusters exhibit modified structural geometry; in the case of $NiZn_{11}O_{12}$, the values of d_{Ni-O}, are (1.825 and 1.826) Å. By investigating the NO

molecule's adsorption on $NiZn_{11}O_{12}$, from Table 2, doping a Zn atom with Ni atom gives highest negative adsorption energy. The $CO/NiZn_{11}O_{12}$ adsorption energy is approximately −1.63 eV, which is approximately 2.5 eV higher than the CO adsorption energy on the pristine cluster. By investigating the NO molecule's adsorption on doping $NiZn_{11}O_{12}$, from Table 2, $NO/NiZn_{11}O_{12}$ gives highest negative adsorption energy (−1.505 eV), which is approximately 2.625 eV higher than the NO adsorption energy on the pristine cluster. We conclude that $Ni–Zn_{11}O_{12}$ nanocage has the potential to improve the accuracy and reliability of hazardous material detection, such as NO and CO.

4.3 The global reactivity parameters

The reactivity parameters estimated using the optimized geometry of DFT / B3LYP–631g(d):

4.3.1 Dipole moment (D)

The dipole moment (D) of a molecule is a crucial factor in determining its reactivity with its surroundings. The dipole moments of the related systems displayed in Tables (1 and 2). The findings show that the polarity of pristine $Zn_{12}O_{12}$ can be relatively weak due to the small value of the dipole moment, with a dipole moment 0.0373D. $Ni/Zn_{12}O_{12}$ has the highest dipole moment, indicating stronger polarization and a greater electrostatic effect on nearby molecules. $NO/NiZn_{12}O_{12}$ comes next, meaning it still has significant polarization but lower than $Ni/Zn_{12}O_{12}$. Meanwhile, $Zn_{12}O_{12}$ decorated with molecules CO and NO separately and $NiZn_{12}O_{12}$ with molecules CO and NO have the lowest dipole moment, suggesting weaker polarization, which could influence its interaction behaviour differently compared to the other two systems. We can see that from the Table 2, $CO/NiZn_{11}O_{12}$ has a higher dipole moment than $NO/NiZn_{11}O_{12}$, indicating that the dipole interaction is stronger in the case of CO adsorption on the surface compared to NO. From the previous data, we found that pristine $Zn_{12}O_{12}$ has the lowest value compared with decorated and dopped states. Higher dipole moment results in stronger electrostatic interactions, leading to more stable adsorption.

4.3.2 Ionization potential IP

Highest IP Value: CO (10.095), meaning it is the most stable in terms of electron loss. Lowest IP Value: $NiZn_{12}O_{12}$ 5.592 indicating it is the most likely to lose electrons. When CO and NO adsorbed on $Zn_{12}O_{12}$ or $NiZn_{12}O_{12}$, the IP changes, increasing or decreasing depending on their interaction with the surface. Introducing Ni into $Zn_{12}O_{12}$ lowers the IP compared to pure $Zn_{12}O_{12}$ (Table 2), suggesting that the system becomes more conductive and less stable in terms

of electron loss. CO is the most stable in terms of electron loss due to its highest IP. $NiZn_{12}O_{12}$ is the least stable as it has the lowest IP. Nickel doping and surface modifications affect ionization potential, altering the electronic properties of the material.

4.3.3 Electrophilic index (ω)

Highest ω Value: $NO/NiZn_{11}O_{12}$ 7.676, meaning they are the most electrophilic and have the highest tendency to attract electrons. Lowest ω Value: CO (3.006), indicating it has the weakest ability to accept electrons. $NO/Zn_{12}O_{12}$ has a high ω value (7.641), showing that NO adsorption on $Zn_{12}O_{12}$ increases electrophilicity significantly. Doping with Ni slightly decreases ω for a part of systems, but CO and NO adsorption on Ni–doped surfaces tends to increase ω, suggesting enhanced electrophilic behaviour. NO adsorption generally increases the electrophilicity of the system. Pure CO has the lowest ω, meaning it is less likely to accept electrons. $NO/NiZn_{11}O_{12}$ and $NO/Zn_{12}O_{12}$ are the most electrophilic (Table 2), making them highly reactive in electron transfer processes.

4.3.5 Chemical hardness (η)

Highest η (most stable system): CO (4.751), meaning it is the hardest and least reactive.

Lowest η (most reactive system): $NO/Zn_{12}O_{12}$ (1.378), suggesting it is highly reactive and easily exchanges electrons. $Zn_{12}O_{12}$ has a relatively high η (2.065), but decreases significantly when NO adsorbed, increasing its reactivity. Doping $Zn_{12}O_{12}$ with Ni reduces η, making the system softer and more reactive, especially after CO and NO adsorption. CO is the most stable system with the highest η, meaning it is least reactive. $NO/Zn_{12}O_{12}$ is the most reactive system with the lowest η. Ni doping reduces chemical hardness (η), making the material more reactive and better suited for catalytic applications.

4.3.4 Electron affinity (EA)

CO is the least likely to accept electrons (lowest EA) (0.593). $Zn_{12}O_{12}$ has a moderate EA (2.855), but its EA increases significantly when NO adsorbed, making it more electrophilic. Nickel doping increases electron affinity, especially when NO or CO adsorbed, (Table 2), improving the system's electrophilicity. $NO/Zn_{12}O_{12}$ (3.211) and $NO/NiZn_{11}O_{12}$ (3.328) are the strongest electron acceptors (highest EA).

4.3.6 Softness (S)

Highest S (most reactive system): $NO/Zn_{12}O_{12}$ (0.363), meaning it is the most reactive and easily exchanges electrons. Lowest S (least reactive system): CO (0.105), indicating it is the hardest and most resistant to electron transfer. $Zn_{12}O_{12}$ has moderate softness (0.242), but NO adsorption increases its softness, making it more reactive. Nickel

doping slightly increases softness, but after CO or NO adsorption, the softness decreases, meaning the system becomes a bit more stable compared to NO/$Zn_{12}O_{12}$, (Table 2). NO/$Zn_{12}O_{12}$ is the softest and most reactive system. CO is the hardest and least reactive system.

4.3.7 Chemical potential (μ)

Highest (least negative) μ (most reactive): $NiZn_{12}O_{12}$ (−4.171), meaning it has the strongest tendency to donate electrons. Lowest (most negative) μ (most stable): CO (−5.344), indicating it is the least reactive and most resistant to electron transfer. $Zn_{12}O_{12}$ has a moderately negative μ (−4.92), but NO adsorption makes it slightly more reactive, (Table 2). Ni–$Zn_{12}O_{12}$ is the most reactive system, as it has the highest μ value. Nickel doping generally increases reactivity, but CO and NO adsorption slightly stabilize the system.

4.4 The frontier molecular orbitals (FMOs):

Energy differences between the lowest unoccupied molecular orbital (LUMO) and the highest occupied molecular orbital (HOMO) are frequently used to measure the electronic properties and chemical reactivity (Fukui, 1982, 218747). These energy gaps are summarized by the theoretical magnitude of the band gap, which determines the transition (excitation) energy between the ground state and the first dipole–allowed excited state (Ashraf and Klemm, 2005, 6445). It is generally known that the reactant molecule's frontier orbitals play an essential role in the chemical reaction, hence the frontier orbital analysis of decorated and doped cages is important. Table 3 summarized the (LUMO and HOMO) surfaces and HOMO–LUMO energy gaps for the $Zn_{12}O_{12}$, CO–$Zn_{12}O_{12}$, NO–$Zn_{12}O_{12}$, Ni–$Zn_{12}O_{12}$, CO/Ni– $Zn_{12}O_{12}$, NO/Ni– $Zn_{12}O_{12}$, Ni– $Zn_{11}O_{12}$, CO/Ni–$Zn_{11}O_{12}$, and CO/Ni–$Zn_{11}O_{12}$ clusters, Figures (3 and 4) presented the related frontier orbital iso surface plots to investigate the effect of adsorbed gases on the adsorbent complexes. $Zn_{12}O_{12}$ energy gap (E_g) of 4.13 eV. The structure in which the CO molecule from its carbon atom is bonded to a Zn atom in the cluster (CO/ $Zn_{12}O_{12}$) has E_g value of 4.128 eV and NO– $Zn_{12}O_{12}$ complex has a reduction in Eg (2.756 eV) when NO molecule is attached, this indicates that the adsorption of NO increases the conductivity of ZnO. After the decoration process, the HOMO level significantly shifted to higher energies, narrowing the E_g of 2.84 eV for Ni–$Zn_{12}O_{12}$ and increasing conductivity (Table 3). When we investigated the CO and NO molecules' adsorption on Ni– $Zn_{12}O_{12}$, It was found that the E_g of CO/Ni– $Zn_{12}O_{12}$ and NO/Ni– $Zn_{12}O_{12}$, decreased from (4.13 eV for $Zn_{12}O_{12}$) into (3.316 and 3.556) eV,

respectively, resulting in increased conductivity and improved electrical characteristics. After the doping process, the HOMO level significantly shifted to higher energies, narrowing the E_g of 3.255 eV for $NiZn_{11}O_{12}$ and increasing conductivity. When we investigated the CO and NO molecules' adsorption on Ni $Zn_{11}O_{12}$, It was found that the $CO/NiZn_{11}O_{12}$ and $NO/Ni\ Zn_{11}O_{12}$ have a reduction in E_g (3.71 and 3.1) eV, respectively, resulting in change in conductivity. The E_g value plays a significant role in defining a material's electrical conductivity (σ). The relationship between a material's E_g and σ can be mathematically stated as follows (Li S., 2006):

$$\sigma \propto exp\left(\frac{-E_g}{2kT}\right) \qquad (12)$$

where k and T are Boltzmann's constant and the temperature, respectively. According to equation Eq. (12), a smaller H–L gap value leads to higher σ at a given temperature T. The electric conductivity of Ni–doped and decorated ZnO structures, in the presence of CO and NO or in the absence of them indicated that the σ for all clusters is higher than that of the $Zn_{12}O_{12}$ cluster.

Understanding the distribution of the frontier orbitals around decorated and doped ZnO would be valuable since it can be employed to guide the improvement of ZnO properties. The charge is concentrated on the cage and another time locate at the pollutants , as seen in Figures (3& 4)). Whereas LUMOs are localized on the surface of nanocage , HOMOs are localized on Ni and pollutants (CO & NO) .This shows a strong electron charge flux across the Ni fragment and ZnO. The charge on Ni at $Ni–Zn_{12}O_{12}$, $CO/Ni–Zn_{12}O_{12}$, $NO/Ni–Zn_{12}O_{12}$, $Ni–Zn_{12}O_{12}$, $CO/NiZn_{11}O_{12}$, and $NO/NiZn_{11}O_{12}$ is 0.437, 0.370, 0.417,0.880,0.686, and 0.204 a.u, respectively, while on the closest neighbors Zn and O are(0.775, –1.140 a.u), (0.969, –1.189 a.u.), (0.495, –0.569 a.u), (1.26,–1.108 a.u), (1.269, –1.126 a.u) and (0.632, –0.560 a.u) respectively, according to our NBO analysis , that shown in Table 2.The d–orbitals of Ni overlap with the p–orbitals of O and the sp^3 orbitals of Zn in the Ni–Zn and Ni–O bonds, indicating that Ni contributes electrons to the nearby Zn and O atoms. Because of this charge transfer behavior, Ni atoms take on a somewhat cationic nature, which makes it easier for Ni to form heteropolar bonds with the surrounding ZnO framework. This interaction alters the electronic structure, increases charge delocalization, and enhances the conductivity of the material.

5. Conclusion

This study explored the role of zinc oxide nanostructures in gas sensing applications, particularly for the detection of carbon monoxide and nitrogen oxide pollutants. Our results highlight that zinc oxide–based

nanomaterials, including doped and decorated clusters, show enormous potential in improving gas sensor efficiency. The computational methods employed, including density functional theory calculations, provided insights into the adsorption mechanisms, energy gaps, and electronic properties. The adsorption energy of Ni – doped and decorated ZnO nanoclusters in the presence of CO and NO gases was –1.63 eV, –1.505 eV, –3.104 eV, and –3.044 eV, respectively, while the energy gaps are 3.71 eV, 3.10 eV, 3.316 eV, and 3.556 eV, respectively. However, in the absence of gases, the energy gaps for each one are 3.255 eV and 2.844 eV, respectively. Among the modifications studied, ZnO nanoclusters decorated with metals such as nickel improved the conductivity and adsorption efficiency. The results indicate that nickel–decorated ZnO offers superior sensitivity and efficiency, making it a promising candidate for sensing applications. Overall, this research emphasizes the importance of material modifications in improving gas sensors. Future studies could explore more dopants and nanostructures to further improve sensor performance and expand its application to broader environmental monitoring challenges.

Acknowledgement

Firstly, we would like to express our gratitude to God for providing us with the strength, wisdom, and perseverance needed to complete this project. We would like to express our deepest gratitude to everyone who supported us throughout the journey of completing this graduation project. First and foremost, we are sincerely thankful to Dr Hayam Osman, whose guidance, encouragement, and insightful feedback were invaluable every step of the way. Your mentorship has greatly contributed to the success of this work. To our professors and academic staff at physics department, thank you for sharing your knowledge and inspiring us throughout our studies. We are also incredibly grateful to our family and friends for their unwavering support, patience, and motivation. We are thankful to everyone who helped with this project, your assistance made this accomplishment possible. Thank you all for being part of this important milestone in our lives.

References and sources:

[1] Zhuiykov S., Wlodarski W., Li Y., (2001), Nanocrystalline V_2O_5–TiO_2 thin–films for oxygen sensing prepared by sol–gel process, Sens Actuators B, 484–490, 77. https://doi.org/10.1016/S0925–4005(01)00739–0

[2] Chang H., Lee J.D., Lee S. M., Lee Y. H., (2001), Adsorption of NH_3 and NO_2 molecules on carbon nanotubes, Appl. Phys. Lett., 3863–3865, 77. https://doi.org/10.1063/1.1424069

[3] Gupta V. K., Nayak A., (2012), Cadmium removal and recovery from aqueous solutions by novel adsorbents prepared from orange peel and Fe_2O_3 nanoparticles. Chem. Eng. J. 81–90, 180. https://doi.org/10.1016/j.cej.2011.11.006.

[4] Mittal A., Kaur D., Malviya A., Mittal J., Gupta V. K., (2009) Adsorption studies on the removal of coloring agent phenol red from wastewater using waste materials as adsorbents. J Colloid Interface Sci, 345–354, 337. https://doi.org/10.1016/j.jcis.2009.05.016.

[5] Ferroni M., Guidi V., Martinelli G., Sacerdoti M., Nelli P., and Sberveglieri G., (1998) MoO_3–based sputtered thin films for fast NO_2 detection, Sensors and Actuators B: Chemical, no. 1–3, 285–288, 48 https://doi.org/10.1016/S0925–4005(98)00057–42–s2.0–0347649437

[6] Sberveglieri G., Depero L., Groppelli S., and Nelli P., (1995), WO_3 sputtered thin films for NOx monitoring, Sensors and Actuators B:Chemical, no.1–3,89–92,26 https://doi.org/10.1016/0925–4005(94)01563–W2–s2.0–0029306414.

[7] Gurlo A., Bârsan N., Ivanovskaya M., Weimar U., and Göpel W., (1998), In_2O_3 and MoO_3–In_2O_3 thin film semiconductor sensors: interaction with NO_2 and O_3, Sensors and Actuators B: Chemical, no.1–3,92–99,47. https://doi.org/10.1016/S0925–4005(98)00033–1,2–s2.0–0347651202.

[8] Santucci S., Picozzi S., Di Gregorio F., Lozzi L., Cantalini C., Valentini L., Kenny J.M., Delley B. (2003) NO_2 and CO gas adsorption on carbon nanotubes: experiment and theory. J Chem Phys (20): 10904–10910, 119. https://doi.org/10.1063/1.1619948

[9] Lee D.S., Han S.D., Huh J.S., Lee D.D. (1999) Nitrogen oxides–sensing characteristics of WO_3–based nanocrystalline thick film gas sensor. Sens Actuators B Chem (1):57–63, 60 https://doi.org/10.1016/S0925–4005(99)00244–0

[10] Peyghan A.A., Baei M.T., Hashemian S., Torabi P., (2013) Adsorption of CO molecule on AlN nanotubes by parallel electric field. J Mol Model 859–870, 19 https://doi.org/10.1007/s00894–012–1614–x

[11] Omaye S.T., (2002) Metabolic modulation of carbon monoxide toxicity. Toxicology 139–150, 180 https://doi.org/10.1016/S0300–483X(02)00387–6

[12] Beheshtian J., Bagheri Z., Kamfiroozi M., Ahmadi A., (2011) Toxic CO detection by B_{12} N_{12} nanocluster. Microelectron J,1400–1403, 42 https://doi.org/10.1016/j.mejo.2011.10.010

[13] Beheshtian J., Kamfiroozi M., Bagheri Z., Ahmadi A. (2011) Computational study of CO and NO adsorption on magnesium oxide nanotubes. Phys E 546–549, 44 https://doi.org/10.1016/j.physe.2011.09.016

[14] Beheshtian J., Peyghan A.A., Bagheri Z., (2012) Selective function of $Al_{12}N_{12}$ nano–cage

towards NO and CO molecules. Comput Mater Sci 71–74, 62 https://doi.org/10.1016/j.commatsci.2012.05.041

[15] Lahmer M.A. (2016) The effect of hydrogen adsorption on the properties of undoped and Cu doped ZnO (100) surfaces: a first–principles study. J Phys Chem Solids 89–96, 89. https://doi.org/10.1016/j.jpcs.2015.10.021

[16] Peyghan A.A., Noei M. (2013) Electronic response of nano–sized cages of ZnO and MgO to presence of nitric oxide. Chin J Chem Phys 231–236, 26. https://doi.org/10.1063/1674–0068/26/02/231–236

[17] Peyghan A.A., Rastegar S.F., Bagheri Z. (2015) Selective detection of F2 in the presence of CO, N_2, O_2, and H_2 molecules using a ZnO nanocluster. MonatshChem1233–1239, 146. https://doi.org/10.1007/s00706–014–1378–3

[18] An W, Wu X., Zeng X.C. (2008) Adsorption of O_2, H_2, CO, NH_3, and NO_2 on ZnO nanotube: a density functional theory study. J Phys Chem C 5747–5755,112. https://doi.org/10.1021/jp711105d

[19] Ü. Özgür, A. YaI, C. Liu et al. (2005) A comprehensive review of ZnO materials and devices. J Appl Phys041301. 98 https://doi.org/10.1063/1.1992666

[20] Beheshtian J., Kamfiroozi M., Bagheri Z., Ahmadi A. (2012) Theoretical study of hydrogen adsorption on the $B_{12}P_{12}$ fullerene–like nanocluster. Compute Mater Sci 115–118, 54. https://doi.org/10.1016/j.commatsci.2011.09.039

[21] Sebastian P.J., Ocampo M., (1996) A photodetector based on ZnCdS nanoparticles in a CdS matrix formed by screen printing and sintering of CdS and $ZnCl_2$. Sol Energy Mater Sol Cells 1–10, 44. https://doi.org/10.1016/0927–0248(95)00168–9

[22] Chakrabarti R., Dutta J., Bandyopadhyay S. et al. (2000) Surface photovoltage measurement in CdS/CdTe solar cell: grain boundary effect. Sol Energy Mater Sol Cells 113–126, 61. https://doi.org/10.1016/S0927–0248(99)00104–X

[23] Gorgani S.S., Nouraliei M. & Gorgani S.S., (2016), Heterogeneous $C_{16}Zn_8O_8$ nanocluster as a selective CO/NO nanosensor, computational investigation, 1573–1580, 13. https://doi.org/10.1007/s13762–016–0973–8

[24]– Yadav M.K., Ghosh M., Biswas R., Raychaudhuri A.K., Mookerjee A., Datta S. (2007) Band–gap variation in Mg– and Cd–doped ZnO nanostructures and molecular clusters. Phys Rev B,195450–195455, 76 https://doi.org/10.1103/PhysRevB.76.195450

[25] Wang B., Nagase S., Zhao J., Wang G. (2007) Structural growth sequences and electronic properties of zinc oxide clusters (ZnO)n (n = 2–18). J Phys Chem C 4956–4963, 111. https://doi.org/10.1021/jp066548v

[26] Reber A.C., Khanna S.N., Hunjan J.S., Beltran M.R. (2007) Rings, towers, cages of ZnO. Eur Phys J D 221–224, 43 https://doi.org/10.1140/epjd/e2007–00087–7

[27] Beheshtian J., Peyghan A.A., Bagheri Z. (2012) Adsorption and dissociation of Cl_2 molecule on ZnO nanocluster. Appl Surf Sci 8171–8176, 258. https://doi.org/10.1016/j.apsusc.2012.05.016

[28] Galstyan V., Comini E., Baratto C., Faglia G., Sberveglieri G. (2015) Nanostructured ZnO chemical gas sensors. Ceram Int (10, Part B):14239–14244, 41. https://doi.org/10.1016/j.ceramint.2015.07.052

[29] Peyghan A.A., Laeen S.P., Aslanzadeh S.A., Moradi M., (2014), Hydrogen peroxide reduction in the oxygen vacancies of ZnO nanotubes. Thin Solid Films, 566–570, 556 https://doi.org/10.1016/j.tsf.2014.01.084

[30] Ameen S., Park D.-R., Shaheer Akhtar M., Shin H.S. (2016) Lotus-leaf like ZnO nanostructures-based electrode for the fabrication of ethyl acetate chemical sensor. Mater Lett 562–566, 164. https://doi.org/10.1016/j.matlet.2015.11.055

[31] Peyghan A.A., Noei M. (2014) The alkali and alkaline earth metal doped ZnO nanotubes: DFT studies. Phys B Condens Matter 105–110, 432. https://doi.org/10.1016/j.physb.2013.09.051

[32] Rocha L.S.R., Foschini C.R., Silva C.C., Longo E., Simões A.Z. (2016) Novel ozone gas sensor based on ZnO nanostructures grown by the microwave-assisted hydrothermal route. Ceram Int 4539–4545, 42. https://doi.org/10.1016/j.ceramint.2015.11.145

[33] Peyghan A.A., Rastegar S.F., Bagheri Z., (2015) Selective detection of F_2 in the presence of CO, N_2, O_2, and H_2 molecules using a ZnO nanocluster. Monatshefte für Chemie-Chem Mon 1233–1239, 146(8). https://doi.org/10.1007/s00706-014-1378-3

[34] Salimi H., Peyghan A.A., Noei M. (2015) Adsorption of formic acid and formate anion on ZnO nanocage: a DFT study. J Clust Sci 609–621, 26(2). https://doi.org/10.1007/s10876-014-0815-0

[35] Shirini F., Abedini M., Zamani S., Fallah Moafi H. (2015) Introduction of W-doped ZnO nanocomposite as a new and efficient nanocatalyst for the synthesis of biscoumarins in water. J Nanostruct Chem 123–130, 5 https://doi.org/10.1007/s40097-014-0143-9

[36] Benramache S., Arif A., Belahssen O., Guettaf A. (2013) Study on the correlation between crystallite size and optical gap energy of doped ZnO thin film. J Nanostruct Chem 1–6, 3. https://doi.org/10.1186/2193-8865-3-80

[37] Hongsith N., Viriyaworasakul C., Mangkorntong P., Mangkorntong N., Choopun S. (2008) Ethanol sensor based on ZnO and Au-doped ZnO nanowires. Ceram Int 823–826, 34. https://doi.org/10.1016/j.ceramint.2007.09.099

[38] Sahay P., Nath R. (2008) Al-doped ZnO thin films as methanol sensors. Sensors Actuators B Chem 654–659, 134(2). https://doi.org/10.1016/j.snb.2008.06.006

[39] Aslanzadeh S., (2016), Transition metal doped ZnO nanoclusters for carbon monoxide detection: DFT studies, 160, 22. https://doi.org/10.1007/s00894-016-3032-y

[40] Kovalenko M., Bovgyra O., Dzikovskyi V. & Rostyslav B., (2020) A DFT study for adsorption of CO and H2 on Pt-doped ZnO nanocluster, 790, 2 (2020). https://doi.org/10.1007/s42452-020-2591-9

[41] An W, Wu X, Zeng XC, (2008) Adsorption of O_2, H_2, CO, NH_3, and NO_2 on ZnO nanotube: a density functional theory study. J Phys Chem C 5747–5755, 112. https://doi.org/10.1021/jp711105d

[42] Zhihong Y., Ye Y., Pejhan A., Nasr A.H., Nourbakhsh N., Tayebee R. (2020). A theoretical study on the pure and doped ZnO nanoclusters as effective nanobiosensors for 5-fluorouracil anticancer drug adsorption 34,4. https://doi.org/10.1002/aoc.5534

[43] Liangruksa M., Sukpoonprom P., Junkaew A., Photaram W., Siriwong C., (2021) Gas sensing properties of palladium-modified zinc oxide nanofilms: A DFT study, Appl. Surf. Sci., 148868, 544. https://doi.org/10.1016/j.apsusc.2020.148868

[44] Frisch M. J., et al.,(2009) Gaussian 09, Revision D.01, Gaussian, Inc., Wallingford, CT.

[45] Becke A. D., (1993) A new mixing of Hartree–Fock and local density functional theories. J. Chem. Phys,1372–1377, 98. https://doi.org/10.1063/1.464304

[46] Ernzerhof M., (2009) Validity of the extended Koopmans' theorem. J. Chem. Theory Comput, 793–797, 5. https://doi.org/10.1021/ct800552k

[47] Islam N., Ghosh D. C., (2011) the electronegativity, and the global hardness are periodic properties of atoms. J. Quantum Inf. Sci.,135–141, 01. https://doi.org/10.4236/jqis.2011.13019

[48] Chattaraj P.K., Roy D. R., (2007) Update 1 of: electrophilicity index, Chem. Rev., 46–79, 107. https://doi.org/10.1021/cr078014b.

[49] Dennington R., Keith T., Millam J., (2009) GaussView, Version 5.0.8.: Semichem Inc., Shawnee Mission KS.

[50] Fukui K., (1982), Role of Frontier Orbitals in Chemical Reactions. Science, 218747. https://doi.org/10.1126/science.218.4574.747.

[51] Ashraf R. S., Klemm E., (2005), Synthesis and properties of poly (heteroaryleneethynylene) consisting of electron-accepting benzothiadiazole/quinoxaline units and electron-donating alkyl thiophene units, J. Polym. Sci. Part A,6445, 43. https://doi.org/10.1002/pola.21089.

[52] Li S., (2006) "*Semiconductor Physical Electronics*", second ed., Springer, USA.